Sub-stochiometric nickel oxide hole selective contacts in solar cells; comparison of simulations and experiments with sputtered films.

Mrutyunjay Nayak[a]*, Kristin Bergum[a], George Stan[b], In-Hwan Lee[c] and Andrej Kuznetsov[a]
[a] *Centre for Materials Science and Nanotechnology, University of Oslo, PO Box 1048, Blindern, N-0316 Oslo, Norway*
[b]*National Institute of Materials Physics, Atomistilor 405A, 077125,Magurele, Ilfov, Romania*
[c]*Department of Materials Science and Engineering, Korea University, Seoul 02841, South Korea*

Abstract

Sub-stochiometric nickel oxide (NiO_x) films were investigated as a hole selective contact option in silicon (Si) heterojunction solar cells. Numerical simulations were carried out to evaluate the impacts of the NiO_x electronic properties variations and the NiO_x/Si interface defect density (D_{it}) on device performance. Simulation data suggest that the best performance is achievable for higher bandgaps (E_g) and corresponding high valence band edge (E_{VB}) positions in the NiO_x films. Overall, in simulations, the performance remains practically unchanged for the nickel vacancy concentrations $[V_{Ni}] = 10^{17} \div 10^{21}$ cm^{-3}, assuming high E_{VB} and low D_{it}. The experimental data measured using NiO_x films prepared by radio-frequency magnetron sputtering reveal that the increase in $[V_{Ni}]$ lifts the conductivity, concurrently decreasing E_g and E_{VB}. As a result, we concluded that the performance of the fabricated sputtered NiO_x/Si heterojunction solar cell is limited by high D_{it} as well as low E_g and E_{VB}.

Keywords: silicon heterojunction solar cells, carrier selective contacts, nickel oxide, simulations, magnetron sputtering.

**Corresponding author: mrutyunjay.nayak@smn.uio.no*

I. Introduction

Transition metal oxides are currently explored as hole /electron selective contact options in silicon (Si) heterojunction solar cells [1]–[11], [12]–[14]. Indeed, negligible parasitic absorption, tunable electronic properties, abundance and low-cost deposition methods make these materials attractive for opto-electronic applications. Importantly, some of the transition metal oxides exhibit *n*-type conductivity due to energetically favorable oxygen (anion) vacancies (*e.g.*, MoO_3, V_2O_5, WO_3, TiO_2); on the other hand, oxides like NiO or Cu_2O behave as *p*-type due to energetically favorable metal cation vacancies [15]. Notably, some oxides (MoO_3, V_2O_5), despite being *n*-type semiconductors behave as good hole selective contacts due to their high work functions [16], [17]. Concurrently, even though *p*-type oxides (Cu_2O, NiO) were expected to work well as hole selective contacts, their practical performance is often found insufficient as compared to competing *n*-type metal oxides [18]–[21]. Indeed, Pramod *et al.* have reported 3.9 % efficiency in the device with sputtered Cu_2O contacts [18]. Further, 5.48 % efficiency was reached by Kurias *et al.* using boron doped-Cu_2O contacts [19]. Xueliang *et al.* reported 4.3 % efficiency with radio-frequency (RF) magnetron sputtered NiO (at a substrate temperature of 300 °C) [20]. Significantly higher efficiency of 10.8 % was reported by Yang *et al.* with the sputtered composite Cu/NiO contacts [22]. So far, the highest efficiency of 17.3 % was reported by Nayak *et al.* with thermally evaporated sub-stoichiometric nickel oxide (NiO_x) [23]. Nevertheless, all these data obtained with *p*-type oxides must be set into comparison with *n*-type oxides having high work functions.

Importantly, the sub-stoichiometry factor may play a prominent role in the engineering of the hole selective contacts since it might affect all key parameters, such as the bandgap (E_g), the valence band edge (E_{VB}) position, the interface states density (D_{it}) and the bulk defect concentration, labelled as [V_{Ni}] for Ni vacancies in NiO_x. For example, Dreon *et al.* [3] have recently reported

23.5% efficient Si heterojunction solar cell using thermally evaporated sub-stoichiometry molybdenum oxide (MoO_x) hole selective layer. Notably, there are reports on magnetron sputtered *n*-type metal oxide-based hole selective contacts in Si heterojunction solar cells showing lower performance in comparison with evaporated films [24], [25]. For this class of contacts, the highest efficiency of 17.5 % was reported recently by Xiufang *et al.* for sputtered MoO_x [26].

Thus, developing suitable *p*-type oxide hole selective contacts is a great challenge in Si photovoltaics. Due to a variety of parameters involved, it is important to carry out numerical simulations to identify the parameter ranges optimal for the device performance, providing a guidance for the growth conditions optimization. In this work, we adopted 1-D numerical simulations to evaluate the impact of the NiO_x electronic properties variations and the NiO_x/Si interface defect density (D_{it}) on the solar cells performance. The simulations were set in the context of the experimental data, interpreting the performance limitation of the RF magnetron sputtered NiO_x/Si heterojunction solar cells.

II. Simulation framework

All device simulations were carried out using AFROS-HET 1-D numerical simulation software (originated from the Helmholtz-Zentrum Berlin) [27]. Some of the parameters used in the simulations were taken from literature [28], [29]. The AM 1.5G solar spectrum is used for evaluating solar cell parameters under illumination.

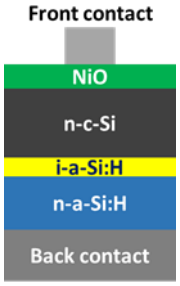

Fig. 1. Schematics of the device structure used in simulations.

The device structure used in the simulations is shown in Fig. 1. The standard electron selective contact consisting of the n-type and intrinsic hydrogenated amorphous silicon (n-a-Si:H/i-a-Si:H) was applied. The interface defect density between n-Si/i-a-Si:H was kept constant at 4.6×10^{10} $cm^{-2}eV^{-1}$ for all simulations. The D_{it} refers to the n-Si/NiO_x interface defect density, which is varied to understand its impact on the band alignment and device performance. The E_{VB} refers to the maximum valence band edge position in NiO_x with respect to the vacuum level. The E_{VB} is varied by varying the NiO_x bandgap (E_g). The electron defect capture cross section (C_n) and hole defect capture cross section (C_p) were kept at 5×10^{-14} cm^2 and 1×10^{-14} cm^2, respectively, in all simulations. The front and back contact boundaries are considered as flat bands. The material parameters used in simulations are listed in Table S1 (see Supplementary information). The E_{VB} value is varied from 4.6 eV to 5.4 eV based on the reported experimental data [30], [31].

III. Experimental details

NiO_x films were deposited on fused silica and *n*-type silicon substrates from a NiO ceramic target by magnetron sputtering at a base pressure of ~1.6×10^{-6} torr, using a 1.58 watt/cm^2 RF power density. The fused silica substrates were cleaned ultrasonically in acetone, IPA and DI water for 15 min each. The cleaned fused silica substrates were dried before transferring into the sputtering chamber for deposition. The *n*-type float zone (FZ) double side polished Si wafers having a doping concentration of ~1.9×10^{15} cm^{-3}, bulk lifetime of ~2 ms, and resistivity of 2 – 3 Ωcm were used for the film deposition and consequent Al/NiO_x/n-Si/Al device fabrication. The silicon wafers were cleaned by piranha followed by the RCA-2 treatment. Notably, the devices were fabricated with a SiO_x interlayer grown after RCA-2 cleaning without applying an HF dip. The dark current voltage

(I-V) characteristics of the fabricated devices were recorded using a Keithley source meter (model no-6487). Injection dependent minority carrier lifetime is measured by Sinton WCT-120 quasi-steady-state photo conductance decay life time measurement system. The optical transmittance of the NiO_x films was monitored by photo spectrometer (Shimadzu SolidSpec-3700 DUV with an integrating sphere). The thickness of the NiO_x films were determined by spectroscopic ellipsometry (J.A Woolam, Alpha SE). The sheet resistance and conductivity of the NiO_x thin films were measured by four-point probe (model: Jandel KM3-AR).

IV. Results and discussion

A. Simulations

Depending on the growth and fabrication condition, electronic and interfacial properties of the hole selective contact may vary instead of being single determined parameters. To illustrate the effect of the multiparameter variations on the device performance, the simulated solar cell parameters are presented in Fig. 2, for different E_{VB} and $[V_{Ni}]$ at low D_{it} =4.6×10^{9} cm^{-2} eV^{-1} assuming NiO_x thickness of 7 nm. The short circuit current density (J_{sc}) remains at ~ 40 mA/cm^2 for both high and low E_{VB} and $[V_{Ni}]$ (see the corresponding characteristics in the Supplementary information, Fig. S1). We acknowledge that J_{sc} varies as a function of the NiO_x thickness due to changing absorption and bulk resistance. However, the thickness is a readily controllable external parameter adjustable during fabrication and we have not considered the NiO_x thickness variation in the simulations. The open circuit voltage (V_{OC}) variations are presented in Fig. 2a. The maximum V_{OC} can be achieved for E_{VB}= 5.2 - 5.4 eV (blue shaded region in the contour plot, Fig.2a). For E_{VB} = 5.2 eV, $[V_{Ni}]$ needs to be $\geq 1\times10^{19}$ cm^{-3}; however, for E_{VB} = 5.4 eV, high V_{OC}

can be achieved even at lower [V_{Ni}] (in the range of 1×10^{17} cm^{-3}). The fill factor (FF) maximum can be achieved for the E_{VB} range of 5.1-5.3 eV, see Fig.2b.

Fig. 2c illustrates realistic ranges of E_{VB} and [V_{Ni}] providing high efficiency; with the maximum efficiency achieved for E_{VB} =5.2 – 5.4 eV. Specifically, at E_{VB} = 5.4 eV, the device efficiency reaches 22.3% with V_{OC}= 702 mV and FF = 79.42 %. Notably, the device performance remains nearly the same for [V_{Ni}] = $1\times10^{17} \div 1\times10^{21}$ cm^{-3}. For lower E_{VB} = 5.2 eV the maximum efficiency can still be achieved at [V_{Ni}] $\geq1\times10^{18}$ cm^{-3}. Further decrease in E_{VB} below 5.2 eV results in the degradation of the device efficiency, associated with a rapid decrease in both V_{OC} and FF. Notably, the carrier collection through *n*-Si/NiO_x hetero-interface might not depend only on the bulk and interface electronic properties of the NiO_x film, but also on the barrier provided by the band offset at the *n*-Si/NiO_x heterojunction. As a result, for high E_{VB}, the valence band may not be optimum for efficient carrier collection due to large valence band offset (ΔE_V) in comparison to low ΔE_V at moderate E_{VB}. The ΔE_V and ΔE_c values of *n*-Si/NiO_x silicon heterojunction for different E_{VB} values are presented in Table I.

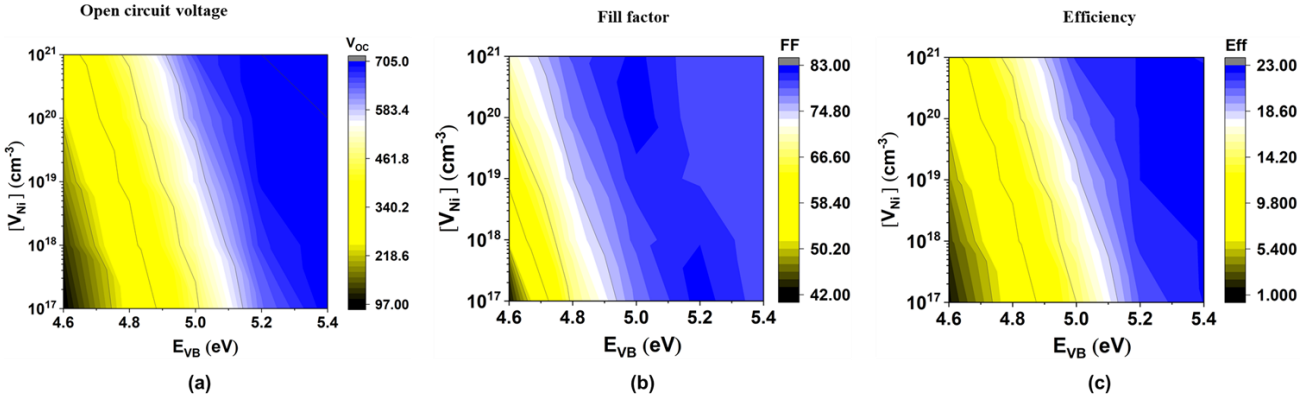

Fig. 2. Impact of the valence band edge position (E_{VB}) and the nickel vacancy concentration [V_{Ni}] on the solar cell in Fig. 1 at D_{it} = 4.6×10^{9} cm^{-2} eV^{-1}: (a) open circuit voltage, (b) fill factor, and (c) efficiency.

The ΔE_V and ΔE_c values are evaluated according to Equations (1) and (2), respectively.

$$\Delta E_v = \left(E_g^{NiO_x} - E_g^{si}\right) - \left(\chi_{si} - \chi_{NiO_x}\right) \quad (1)$$

$$\Delta E_c = \left(\chi_{si} - \chi_{NiO_x}\right) \quad (2)$$

Where; χ is the electron affinity and E_g is the band gap.

Table I. ΔE_V and ΔE_c values of the n-Si/NiO_x silicon heterojunction as a function of E_{VB} as calculated from Equations (1) and (2).

E_{VB} (eV)	ΔE_v (eV)	ΔE_c (eV)
5.4	0.23	2.25
5.2	0.03	2.25
5.0	-0.17	2.25
4.8	-0.37	2.25
4.6	-0.57	2.25

The simulated energy band diagrams of the NiO_x/n-Si silicon heterojunction solar cell under dark and light conditions are presented in Fig. 3. These data help to understand the impact of the band alignment and ΔE_V on V_{OC}, FF and efficiency. The conduction band offset $\Delta E_c \geq 2$ eV at the NiO_x/n-Si silicon heterojunction is sufficient to block the majority carriers (electrons), therefore, we have not extended our explanation to the variation in ΔE_c. The line diagram of the NiO_x/n-Si silicon heterojunction, showing ΔE_V and ΔE_C is presented in Supplementary information in Fig. S3.

For n-type silicon heterojunction solar cell, the minority carriers (holes) generated under illumination are directed towards the hole contact. High ΔE_V in the front junction (n-Si/hole

selective contact) may enroll transport barrier to the holes, resulting in lowering of the device efficiency. Such barriers due to large ΔE_V reduce the carrier flow by thermal emission and increase the tunneling transport through hopping via valence band tail states [32]. This scenario is also observed in c-Si/a-Si heterojunction solar cells, the ΔE_V may vary in the range of 0.2-0.45 eV [32]. As seen from Fig. 3 for E_{VB} = 5.2 eV the ΔE_V is low (0.03 eV), while for E_{VB} = 5.4 eV, ΔE_V increases to 0.23 eV. The increase in ΔE_V from 0.03 eV to 0.23 eV reduces the FF from 82.4% to 79.4%. However, the V_{OC} increases from 635 mV to 702 mV if changing E_{VB} from 5.2 eV to 5.4 eV. This is also reflected in the quasi-Fermi level splitting (E_{Fn}-E_{Fp}) under light in the energy band diagram (Fig. 3c, Fig. 3d). The E_{Fn}-E_{Fp} is bigger for E_{VB} = 5.4 eV compared to E_{VB} = 5.2 eV. As such, there is a tradeoff between V_{OC} and FF as a function of E_{VB}. As a result, moderate E_{VB} in the range of 5.1 – 5.3 eV in combination with enhanced [V_{Ni}] provide the best performance. Concurrently, the variation in [V_{Ni}] also affect the bandgap (E_g), absorption properties [31], [33], [34] and E_{VB} position [31]. However, low D_{it} and [V_{Ni}] $\geq 1\times1^{18}$ cm^{-3}, can provide more flexibility to tune the E_{VB} in the range of 5.1 eV to 5.3 eV without decreasing the device performance. It is also experimentally more feasible to fabricate NiO_x hole selective layer having a window for E_{VB}

optimization. The role of [V_{Ni}] on electronic properties and performance of the device will be elaborated in experimental results section.

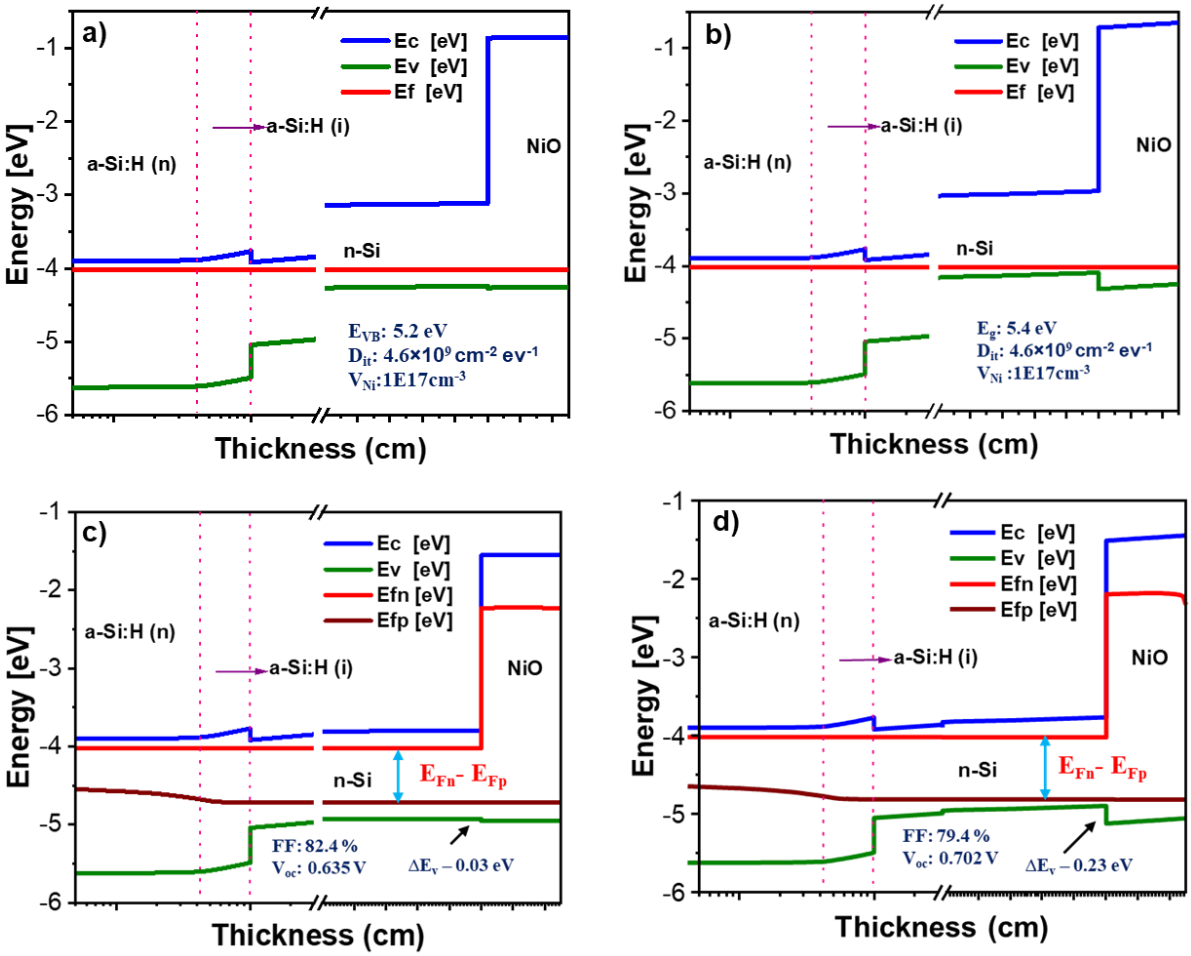

Fig. 3. Simulated energy band diagram of the n-Si/NiO_x heterojunction solar cell at fixed D_{it} = 4.6×10^{9} cm^{-2} eV^{-1} and [V_{Ni}] = 1×10^{17} cm^{-3}: (a) under dark with E_{VB} = 5.2 eV, (b) under dark with E_{VB} = 5.4 eV, (c) under light with E_{VB} = 5.2 eV and (d) under light with E_{VB} = 5.4 eV.

The interface defect density also plays an important role in the device performance[35], [36]. The effects of high D_{it} (4.6×10^{13} cm^{-2} eV^{-1}) on the solar parameters are presented in Fig. 4 for simultaneous variations of E_{VB} and [V_{Ni}]. With increase in D_{it} from 4.6×10^{9} cm^{-2} eV^{-1} to 4.6×10^{13} cm^{-2} eV^{-1}, the window of E_{VB} and [V_{Ni}] optimum values become narrow; *e.g.*, maximum

achievable V_{OC} does not exceed ~650 mV (Fig. 4a). Similarly, for FF (Fig. 4b) and efficiency (Fig. 4c), optimum values also shift to a very narrow range even at maximum E_{VB} and V_{Ni}.

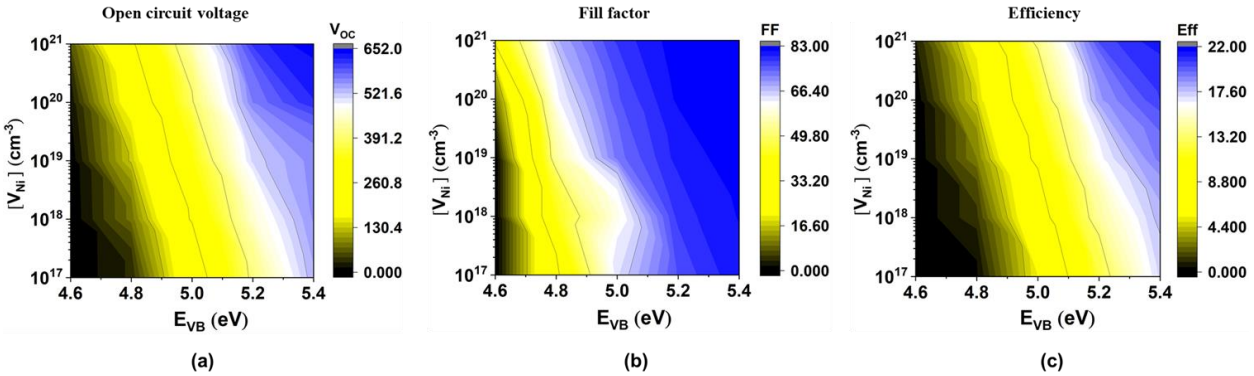

Fig. 4. Illustration of the device performance modifications while changing from low Dit (as in Fig. 2) to $D_{it} = 4.6\times10^{13}$ $cm^{-2.}$

For n-Si heterojunction, the open circuit voltage (V_{OC}) can be expressed in terms of D_{it} and effective barrier height (Φ_B) as

$$V_{OC}(SHJn) = \frac{\varphi_B}{q} - \frac{nkT}{q}\ln\left(\frac{qN_vC_pD_{it}}{J_{sc}}\right) \qquad (3)$$

Where; the C_p is the hole defect capture coefficient, n is the diode ideality factor, q is the electron charge, N_v is the effective valence band density of states, k is the Boltzmann constant, and T is the temperature[35]. Notably, Cp is kept constant for all simulations. The barrier height of the device depends on the band alignment and work function difference between n-Si and NiO_x. The overall band bending and barrier height decreases with the D_{it} increase in according to the Equation (3); due to pinning of the Fermi level. Notably, this is reflected in the simulated light J-V characteristics (Supplementary information, Fig. S2). The corresponding device performance degrades (compare

Figs. 2 and 4,) with the V_{OC} and efficiency decreasing from 704 mV to 588 mV and 22.3% to 19.3 %, respectively.

B. Data obtained with sputtered NiO_x films

Fig. 5 summarizes the data collected from magnetron sputtered NiO_x films deposited on fused silica and n-Si substrates to experimentally evaluate the variations in the optical and electrical properties. The transmittance spectra and the corresponding Tauc plots are presented in Fig. 5a. The transmittance decreases and the band gap also decreases (see the Fig. 5a) when adding oxygen in the sputtering chamber. The decrease in transmittance and bandgap is due to increasing $[V_{Ni}]$ as a function of the oxygen flow due to the sub-bandgap absorption facilitated by the defect states created by V_{Ni} [31], [33]. The increase in $[V_{Ni}]$ with increase in oxygen flow also shifts the valence band maximum position upward towards vacuum level and decrease the E_{VB} [31].

The sheet resistance (R_{sh}) and conductivity ($\boldsymbol{\sigma}$) data are presented in Table II. The R_{sh} decreases from 15.8 (MΩ/□) to 145.5 (kΩ/□) and conductivity is improved to one order (from 4.9×10^{-1} 1/Ω-cm to 4.9 1/Ω-cm) with oxygen flow.

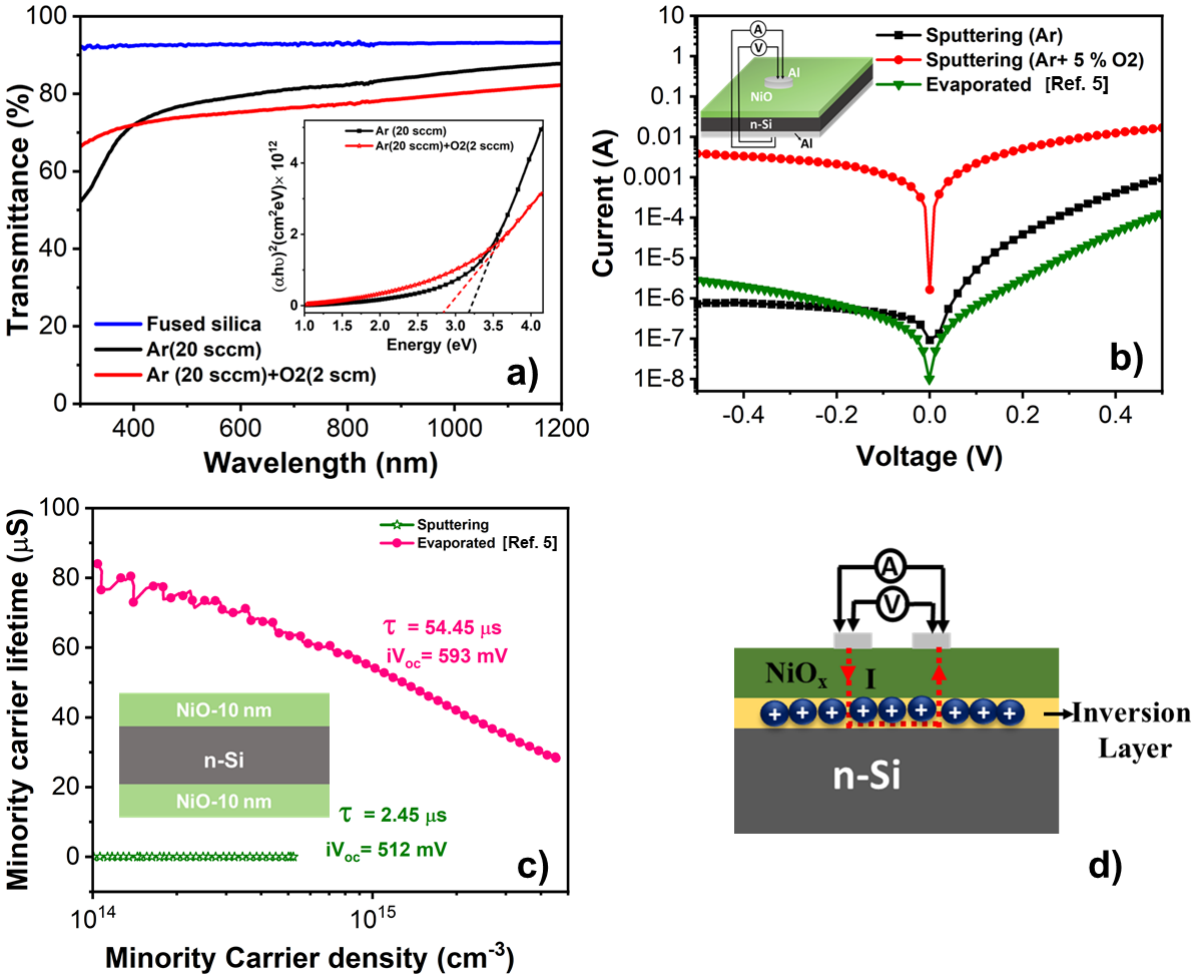

Fig. 5. Summary of the experimental data collected to evaluate electronic and optical properties of the devices (a) transmittance of the NiO_x films with and without oxygen flow. Tauc plot is shown in the inset, (b) dark J-V characteristics of the n-Si/NiO_x heterojunction; Schematic of the diode structure is shown in the inset, (c) minority carrier lifetime vs minority carrier density of the sputtered NiO_x; the minority carrier life time test structure is shown in the inset and (d) schematics of the current path through the inversion layer induced in n-Si. The evaporated NiO_x film minority carrier life time and dark current density-voltage data are taken from Ref. [5] for comparison.

Table II. The sheet resistance and conductivity of the NiO_x films used to collect data in Fig. 5.

NiO_x	R_{sh} (On Fused silica)	σ (1/Ω-cm)	R_{sh} (on n-Si)
15 nm (Ar 20 sccm)	15.8 (MΩ/□)	4.9×10^{-1}	53.91(Ω/□)
15 nm (Ar-20 sccm+ O_2-2 sccm)	145.5 (kΩ/□)	4.9	389.2(Ω/□)

The performance of the sputtered NiO_x/n-Si heterojunction is evaluated by measuring the dark I-V characteristics of the NiO_x/n-Si heterojunction diode as shown in Fig. 5b. The fabricated diode structure is shown in the inset of Fig. 5b. The diode fabricated with NiO_x film by adding oxygen shows very poor performance compared to the NiO_x film with pure argon. This reflects increase in V_{Ni} due to addition of oxygen not only affect the transmittance and E_g, but also affect the band bending, barrier height and performance of the device. The J-V characteristics of the device with the NiO_x films sputtered in pure ~~oxygen~~ argon is better, but still less good comparing with the literature data for thermally-evaporated films [5].

Radically better performance of the thermal evaporated NiO_x/n-Si devices reflects growth condition also significantly affect the electronic properties and performance of the device. The minority carrier density *vs.* minority carrier life time data of sputtered NiO_x film is measured and compared with the data of thermally evaporated one (shown in the Fig. 5c) to understand the effect of growth conditions on the performance of the device. The lifetime test structure used for measurement is shown in the inset of Fig. 5c. Low minority carrier life time of 2.45 µs indicates high surface recombination due to the interface defects [37]. In contrast, lifetime data for the evaporated NiO_x film show better minority carrier life time of 54.45 µs [5]. The interface passivation depends on both chemical passivation and field effect passivation. The very thin (~2 nm) interfacial SiO_x layer provides some chemical passivation [38], [39] and the high work function of NiO_x film results in field effect passivation with an induced inversion layer [40], [41]. Poor minority carrier life time of the sputtered NiO_x film test structure may be due to the additional defects created by plasma during sputtering [42], [43]. This may also affects the work function of the NiO_x film, and further reduce the field effect passivation [44]–[46].

Further comparison of the R_{sh} data for the NiO_x films deposited on n-Si results in a paradoxical observation: nominally less resistive NiO_x film obtained by adding oxygen shows higher R_{sh} value comparing to that deposited in argon only (see the data in Table II). The NiO_x film with high work function induces an inversion layer at the NiO_x/n-Si interface [41] and provides low resistive current path as shown in Fig. 5d. The high R_{sh} value (389.2 Ω/□) of the more conducting NiO_x film grown with addition of oxygen compared to the NiO_x film obtained with pure argon (53.91 Ω/□) is interconnected with high [V_{Ni}], lowering the band bending, creating a poor inversion layer and providing more resistive path. This is also reflected in the poor performance of the dark J-V characteristics in Fig. 5b for the sample prepared with the addition of oxygen to the sputtering chamber.

V. Conclusions

Sub-stochiometric NiO_x hole selective contacts were investigated for the use in silicon heterojunction solar cells. The impacts of the NiO_x bulk electronic properties and NiO_x/n-Si interface defect density (D_{it}) variations on the NiO_x/n-Si heterojunction solar cell band alignment and performance were evaluated using numerical simulations. Higher bandgaps (E_g) and high valence band edge (E_{VB}) positions of the NiO_x film result in the optimal performance. The increase in D_{it} degrades the performance of the device, and the degradation rate is more severe at low E_{VB}. The nickel vacancy concentration [V_{Ni}] variations in the $10^{17} \div 10^{21}$ cm^{-3} range does not affect the performance of the device at high E_{VB} and low D_{it}. On the other hand, E_{VB} lowering degrades the performance of the device. The valence band offset (ΔE_V) at the NiO_x/n-Si hetero interface affects the carrier transport and fill factor of the device. Higher [V_{Ni}] and low D_{it} provides more flexibility to tune the E_{VB} with minimum ΔE_V to achieve best performance of the device. The conductivity increases with increase in V_{Ni} concentration, concurrently decreasing E_g/E_{VB}. Thus, high D_{it} as

well as low E_g and E_{VB} limits the performance of the fabricated sputtered NiO_x/n-Si heterojunction diode.

Acknowledgements

The research leading to these results has received funding from the EEA Grants 2014–2021, under Project contract no. 36/2021 (project code: EEA-RO-NO-2018-0106). The Research Council of Norway is acknowledged for the support to the Norwegian Micro- and Nano-Fabrication Facility, NorFab, project number 295864. The international collaboration was enabled by the INTPART program at the research council of Norway (project No. 261574 and no. 322382).

References

[1] J. Bullock *et al.*, "Efficient silicon solar cells with dopant-free asymmetric heterocontacts," *Nature Energy*, vol. 1, no. 3, p. 15031, Mar. 2016, doi: 10.1038/nenergy.2015.31.

[2] J. Geissbühler *et al.*, "22.5% Efficient Silicon Heterojunction Solar Cell With Molybdenum Oxide Hole Collector," *Applied Physics Letters*, vol. 107, no. 8, p. 081601, Aug. 2015, doi: 10.1063/1.4928747.

[3] J. Dréon *et al.*, "23.5%-Efficient Silicon Heterojunction Silicon Solar Cell Using Molybdenum Oxide As Hole-Selective Contact," *Nano Energy*, vol. 70, p. 104495, Apr. 2020, doi: 10.1016/j.nanoen.2020.104495.

[4] J. Bullock *et al.*, "Dopant-Free Partial Rear Contacts Enabling 23% Silicon Solar Cells," *Advanced Energy Materials*, vol. 9, no. 9, p. 1803367, Mar. 2019, doi: 10.1002/aenm.201803367.

[5] M. Nayak, S. Mandal, A. Pandey, S. Mudgal, S. Singh, and V. K. Komarala, " Nickel Oxide Hole-Selective Heterocontact for Silicon Solar Cells: Role of SiO x Interlayer on Device Performance ," *Solar RRL*, vol. 3, no. 11, p. 1900261, Nov. 2019, doi: 10.1002/solr.201900261.

[6] C. Battaglia *et al.*, "Hole Selective MoO x Contact for Silicon Solar Cells," *Nano Letters*, vol. 14, no. 2, pp. 967–971, Feb. 2014, doi: 10.1021/nl404389u.

[7] M. Xue *et al.*, "Contact Selectivity Engineering in a 2 μm Thick Ultrathin c-Si Solar Cell Using Transition-Metal Oxides Achieving an Efficiency of 10.8%," *ACS Applied Materials and Interfaces*, vol. 9, no. 48, pp. 41863–41870, Dec. 2017, doi: 10.1021/acsami.7b12886.

[8] G. Gregory *et al.*, "Spatial Atomic Layer Deposition of Molybdenum Oxide for Industrial Solar Cells," *Advanced Materials Interfaces*, vol. 7, no. 22, pp. 1–9, 2020, doi: 10.1002/admi.202000895.

[9] G. Gregory, C. Feit, Z. Gao, P. Banerjee, T. Jurca, and K. O. Davis, "Improving the Passivation of Molybdenum Oxide Hole-Selective Contacts with 1 nm Hydrogenated Aluminum Oxide Films for Silicon Solar Cells," *Physica Status Solidi (A) Applications and Materials Science*, vol. 217, no. 15, pp. 1–7, 2020, doi: 10.1002/pssa.202000093.

[10] X. Yang, K. Weber, Z. Hameiri, and S. De Wolf, "Industrially feasible, dopant-free, carrier-selective contacts for high-efficiency silicon solar cells," *Progress in Photovoltaics: Research and Applications*, vol. 25, no. 11, pp. 896–904, Nov. 2017, doi: 10.1002/pip.2901.

[11] M. Nayak, K. Singh, S. Mudgal, S. Mandal, S. Singh, and V. K. Komarala, "Carrier-Selective Contact Based Silicon Solar Cells Processed at Room Temperature using

Industrially Feasible Cz Wafers," *Physica Status Solidi (A) Applications and Materials Science*, vol. 216, no. 16, p. 1900208, Aug. 2019, doi: 10.1002/pssa.201900208.

[12] X. Yang, P. Zheng, Q. Bi, and K. Weber, "Silicon heterojunction solar cells with electron selective TiOx contact," *Solar Energy Materials and Solar Cells*, vol. 150, pp. 32–38, Jun. 2016, doi: 10.1016/j.solmat.2016.01.020.

[13] J. Cho *et al.*, "Passivating electron-selective contacts for silicon solar cells based on an a-Si:H/TiO x stack and a low work function metal," *Progress in Photovoltaics: Research and Applications*, vol. 26, no. 10, pp. 835–845, Oct. 2018, doi: 10.1002/pip.3023.

[14] Y. Zheng *et al.*, "Optimization of SnO2-based electron-selective contacts for Si/PEDOT:PSS heterojunction solar cells," *Solar Energy*, vol. 193, pp. 502–506, Nov. 2019, doi: 10.1016/j.solener.2019.09.077.

[15] M. T. Greiner and Z. H. Lu, "Thin-film metal oxides in organic semiconductor devices: Their electronic structures, work functions and interfaces," *NPG Asia Materials*, vol. 5, no. 7, pp. e55–e55, Jul. 2013, doi: 10.1038/am.2013.29.

[16] J. Melskens, B. W. H. van de Loo, B. Macco, L. E. Black, S. Smit, and W. M. M. Kessels, "Passivating Contacts for Crystalline Silicon Solar Cells: From Concepts and Materials to Prospects," *IEEE Journal of Photovoltaics*, vol. 8, no. 2, pp. 373–388, Mar. 2018, doi: 10.1109/JPHOTOV.2018.2797106.

[17] S. Bhatia, A. Antony, and P. R. Nair, "Unraveling the Hole-Selective Nature of Si/MoOXHeterojunction," *IEEE Journal of Photovoltaics*, vol. 10, no. 6, pp. 1566–1573, Nov. 2020, doi: 10.1109/JPHOTOV.2020.3019957.

[18] P. Ravindra, R. Mukherjee, and S. Avasthi, "Hole-Selective Electron-Blocking Copper Oxide Contact for Silicon Solar Cells," *IEEE Journal of Photovoltaics*, vol. 7, no. 5, pp.

1278–1283, Sep. 2017, doi: 10.1109/JPHOTOV.2017.2720619.

[19] K. K. Markose *et al.*, "Novel Boron-Doped p-Type Cu 2 O Thin Films as a Hole-Selective Contact in c-Si Solar Cells," *ACS Applied Materials & Interfaces*, vol. 12, no. 11, pp. 12972–12981, Mar. 2020, doi: 10.1021/acsami.9b22581.

[20] X. Yang, J. Guo, Y. Zhang, W. Liu, and Y. Sun, "Hole-selective NiO:Cu contact for NiO/Si heterojunction solar cells," *Journal of Alloys and Compounds*, vol. 747, pp. 563–570, May 2018, doi: 10.1016/j.jallcom.2018.03.067.

[21] F.-H. Hsu *et al.*, "Enhanced carrier collection in p-Ni1−xO:Li/n-Si heterojunction solar cells using LiF/Al electrodes," *Thin Solid Films*, vol. 573, pp. 159–163, Dec. 2014, doi: 10.1016/j.tsf.2014.11.025.

[22] X. Yang, W. Liu, J. Chen, and Y. Sun, "On the annealing-induced enhancement of the interface properties of NiO:Cu/wet-SiOx/n-Si tunnelling junction solar cells," *Applied Physics Letters*, vol. 112, no. 17, p. 173904, Apr. 2018, doi: 10.1063/1.5026135.

[23] M. Nayak, A. Pandey, S. Mandal, and V. K. Komarala, "Nickel oxide-based hole-selective contact silicon heterojunction solar cells," 2022, p. 020015, doi: 10.1063/5.0089230.

[24] P. K. Parashar and V. K. Komarala, "Sputter deposited sub-stochiometric MoOx thin film as hole-selective contact layer for silicon based heterojunction devices," *Thin Solid Films*, vol. 682, pp. 76–81, Jul. 2019, doi: 10.1016/j.tsf.2019.05.004.

[25] M. Bivour, F. Zähringer, P. Ndione, and M. Hermle, "Sputter-deposited WOx and MoOx for hole selective contacts," *Energy Procedia*, vol. 124, pp. 400–405, Sep. 2017, doi: 10.1016/j.egypro.2017.09.259.

[26] X. Yang *et al.*, "Sub-stochiometric MoO x by RF magnetron sputtering as hole-selective

passivating contacts for silicon heterojunction solar cells," *Chinese Physics B*, Mar. 2022, doi: 10.1088/1674-1056/ac5a42.

[27] R. Varache, C. Leendertz, M. E. Gueunier-Farret, J. Haschke, D. Muñoz, and L. Korte, "Investigation of selective junctions using a newly developed tunnel current model for solar cell applications," *Solar Energy Materials and Solar Cells*, vol. 141, pp. 14–23, Oct. 2015, doi: 10.1016/j.solmat.2015.05.014.

[28] M. Tan, S. Zhong, W. Wang, and W. Shen, "Silicon homo-heterojunction solar cells: A promising candidate to realize high performance more stably," *AIP Advances*, vol. 7, no. 8, p. 085016, Aug. 2017, doi: 10.1063/1.4993677.

[29] R. Islam, K. N. Nazif, and K. C. Saraswat, "Si Heterojunction Solar Cells: A Simulation Study of the Design Issues," *IEEE Transactions on Electron Devices*, vol. 63, no. 12, pp. 4788–4795, Dec. 2016, doi: 10.1109/TED.2016.2613057.

[30] D. Kawade, S. F. Chichibu, and M. Sugiyama, "Experimental determination of band offsets of NiO-based thin film heterojunctions," *Journal of Applied Physics*, vol. 116, no. 16, p. 163108, Oct. 2014, doi: 10.1063/1.4900737.

[31] J. Keraudy *et al.*, "Process- and optoelectronic-control of NiOx thin films deposited by reactive high power impulse magnetron sputtering," *Journal of Applied Physics*, vol. 121, no. 17, p. 171916, May 2017, doi: 10.1063/1.4978349.

[32] M. Mews, M. Liebhaber, B. Rech, and L. Korte, "Valence band alignment and hole transport in amorphous/crystalline silicon heterojunction solar cells," *Applied Physics Letters*, vol. 107, no. 1, p. 013902, Jul. 2015, doi: 10.1063/1.4926402.

[33] K. O. Egbo, C. P. Liu, C. E. Ekuma, and K. M. Yu, "Vacancy defects induced changes in the electronic and optical properties of NiO studied by spectroscopic ellipsometry and

first-principles calculations," *Journal of Applied Physics*, vol. 128, no. 13, p. 135705, Oct. 2020, doi: 10.1063/5.0021650.

[34] M. L. Grilli *et al.*, "Effect of growth parameters on the properties of RF-sputtered highly conductive and transparent p-type NiO x films," *Semiconductor Science and Technology*, vol. 31, no. 5, p. 055016, May 2016, doi: 10.1088/0268-1242/31/5/055016.

[35] N. Jensen *et al.*, "Recombination mechanisms in amorphous silicon/crystalline silicon heterojunction solar cells," *Journal of Applied Physics*, vol. 87, no. 5, pp. 2639–2645, Mar. 2000, doi: 10.1063/1.372230.

[36] D. Adachi, J. L. Hernández, and K. Yamamoto, "Impact of carrier recombination on fill factor for large area heterojunction crystalline silicon solar cell with 25.1% efficiency," *Applied Physics Letters*, vol. 107, no. 23, p. 233506, Dec. 2015, doi: 10.1063/1.4937224.

[37] R. S. Bonilla and P. R. Wilshaw, "On the c-Si/SiO2 interface recombination parameters from photo-conductance decay measurements," *Journal of Applied Physics*, vol. 121, no. 13, p. 135301, Apr. 2017, doi: 10.1063/1.4979722.

[38] H. Angermann, "Conditioning of Si-interfaces by wet-chemical oxidation: Electronic interface properties study by surface photovoltage measurements Dedicated to Dr. Kurt Heilig on occasion of his 85th birthday.," *Applied Surface Science*, vol. 312, pp. 3–16, Sep. 2014, doi: 10.1016/j.apsusc.2014.05.087.

[39] L. G. Gerling, G. Masmitja, P. Ortega, C. Voz, R. Alcubilla, and J. Puigdollers, "Passivating/hole-selective contacts based on V2O5/SiOx stacks deposited at ambient temperature," *Energy Procedia*, vol. 124, pp. 584–592, Sep. 2017, doi: 10.1016/j.egypro.2017.09.294.

[40] L. G. Gerling, C. Voz, R. Alcubilla, and J. Puigdollers, "Origin of passivation in hole-

selective transition metal oxides for crystalline silicon heterojunction solar cells," *Journal of Materials Research*, vol. 32, no. 2, pp. 260–268, Jan. 2017, doi: 10.1557/jmr.2016.453.

[41] "Physica Rapid Research Ltrs - 2017 - Sun - Investigation of MoOx n-Si strong inversion layer interfaces via dopant-free (1).pdf." .

[42] K. Onishi *et al.*, "Evaluation of plasma induced defects on silicon substrate by solar cell fabrication process," *Japanese Journal of Applied Physics*, vol. 59, no. 7, p. 071003, Jul. 2020, doi: 10.35848/1347-4065/ab984d.

[43] I. Umezu, K. Kohno, K. Aoki, Y. Kohama, A. Sugimura, and M. Inada, "Effects of argon and hydrogen plasmas on the surface of silicon," *Vacuum*, vol. 66, no. 3–4, pp. 453–456, 2002, doi: 10.1016/S0042-207X(02)00170-7.

[44] Y.-J. Lin *et al.*, "Changes in surface roughness and work function of indium-tin-oxide due to KrF excimer laser irradiation," *Journal of Vacuum Science & Technology A: Vacuum, Surfaces, and Films*, vol. 23, no. 5, pp. 1305–1308, Sep. 2005, doi: 10.1116/1.1953670.

[45] T. Kamioka, Y. Hayashi, Y. Isogai, K. Nakamura, and Y. Ohshita, "Analysis of interface workfunction and process-induced damage of reactive-plasma-deposited ITO/SiO 2 /Si stack," *AIP Advances*, vol. 7, no. 9, p. 095212, Sep. 2017, doi: 10.1063/1.4997495.

[46] S. Gutmann, M. A. Wolak, M. Conrad, M. M. Beerbom, and R. Schlaf, "Effect of ultraviolet and x-ray radiation on the work function of TiO2 surfaces," *Journal of Applied Physics*, vol. 107, no. 10, p. 103705, May 2010, doi: 10.1063/1.3410677.